JOURNAL OF PHYSICS B: ATOMIC, MOLECULAR AND OPTICAL PHYSICS 45 (2012): 194008

DOI: http://dx.doi.org/10.1088/0953-4075/45/19/194008

Vibrationally-resolved photoelectron angular distributions from randomly-oriented and fixed-in-space N_2 and CO molecules

E Plésiat[1], P Decleva[2], and F Martín[1,3]

[1]Departamento de Química, Módulo 13, Universidad Autónoma de Madrid, 28049 Madrid, Spain

[2]Dipartimento di Scienze Chimiche, Universitá di Trieste, 34127 Trieste, and CNR-IOM, Trieste, Italy

[3]Instituto Madrileño de Estudios Avanzados en Nanociencia (IMDEA-Nanociencia), Cantoblanco, 28049 Madrid, Spain

E-mail: `fernando.martin@uam.es`

Abstract. Vibrationally resolved photoelectron angular distributions from randomly oriented and fixed-in-space N_2 and CO molecules have been evaluated by using an extension of the static-exchange density functional theory that includes the nuclear motion. Both K-shell and valence-shell photoionization have been considered. Comparison with the experimental data, only available for randomly oriented molecules, is very good. Our predictions for molecular-frame photoelectron angular distributions of N_2 show the signature of electron confinement and coherent two-center interferences as those previously found in H_2. For CO, they exhibit diffraction patterns associated with the scattering of the ejected electron by the neighboring atomic center. The conclusions reported in this work suggest that vibrationally resolved photoelectron angular distributions can be a useful instrument to determine structure parameters in these simple molecules.

PACS numbers: 34.10.+x, 31.10.+z, 33.60.+q, 33.20.Wr

1. Introduction

Photoionization of simple diatomic molecules, in particular N_2 and CO, is a subject that has received continuous attention since the early 1960's. This fundamental process is often the benchmark for new theoretical developments, which are necessary to account for the meV accuracy of photoelectron spectra currently available. Until recently, most experimental and theoretical investigations in N_2 and CO have focused on obtaining and understanding total photoelectron spectra corresponding to core- as well as valence-shell photoionization (see, e.g., [1–3] and references therein), from the ionization threshold up to a few tens of eV above it. More recently, with the advent of high-brilliance 3rd-generation synchrotron radiation sources in combination with high energy-resolution detection techniques, determination of vibrationally resolved photoionization spectra

has become accessible [4–14], which has fostered the development of theoretical methods that also account for molecular vibrations [3, 8–11, 13, 15–23].

Evaluation of total photoelectron spectra is relatively straightforward since, for this, it is reasonable to assume that the nuclei are fixed at their equilibrium positions (the fixed-nuclei approximation). Obviously, this assumption is no longer valid to evaluate vibrationally resolved cross sections, since one also needs the electronic wave functions outside the equilibrium positions to account for the nuclear motion in the potential created by the electrons. This makes calculations significantly more expensive, hence applications are scarcer, as the electronic structure must be determined for many molecular geometries, including the equilibrium one used in the fixed-nuclei approximation. For the same reason, there exist few theoretical works that have provided vibrationally resolved (or ion-energy resolved) electron angular distributions, either for randomly oriented [10, 13, 18, 24–29] or fixed-in-space N_2 and CO molecules. Furthermore, most of them have focused on the low-energy region. In contrast, the amount of experimental information on vibrationally resolved angular distributions is relatively abundant (see [4, 5, 10, 13, 18, 24–38] and references therein).

Recent work on vibrationally resolved photoelectron spectra at high energies has shown [3, 21]: (i) two-center coherent electron emission leading to Young's type double-slit interferences [39] and (ii) electron diffraction by the molecule's atomic centers. These processes are possible because, at high photon energy, the wavelength λ_e of the ejected electron is comparable to or smaller than the size of the molecule [40, 41]. The main experimental difficulty is to extract the relatively small diffraction features from the rapidly decreasing cross section as a function of photoelectron energy. The latter difficulty was overcome in [3, 21] by taking the ratios of vibrationally resolved photoelectron spectra. In Refs. [40, 42], it has been shown that, for the H_2 molecule, such interferences become even more apparent in vibrationally-resolved molecular-frame photoelectron angular distributions, MFPAD (or vibrationally-resolved photoelectron angular distributions from fixed-in-space molecules). In particular, for H_2 molecules perpendicular to the polarization direction, the MFPADs clearly resemble the interferences seen in the classical Young's double-slit experiment, while, for molecules parallel to the polarization direction, they show that the electron is sometimes prevented from escaping in the direction of the radiation electric field due to the suppression of a given partial wave. The latter effect has not been observed in the MFPADs of other molecules, while there is already strong evidence that two-center interference effects also leave their signature in the MFPADs resulting from dissociative photoionization of N_2 and CO [37, 43–46].

In this paper we present vibrationally-resolved photoelectron angular distributions for both randomly oriented (i.e., β parameters) and fixed-in-space (i.e., MFPADs) N_2 and CO molecules, at low and high energies, and for both core and valence-shell orbitals. We show that effects similar to those previously reported in [40, 42] are also observed in the MPFADs of N_2 and CO. The paper is organized as follows. In section 2 we describe in detail the static-exchange density functional theory (DFT) including nuclear

vibrations that has been used in the present work. The results are presented in section 3. Vibrationally resolved β parameters are discussed in section 3.1, where they are compared with the few available experimental data. In section 3.2 we present the MFPADs at high photon energies and we discuss the origin of the different interferences observed in these distributions. Conclusions are given in section 4.

2. Theory

The vibrationally resolved photoionization amplitudes are evaluated to first order of perturbation theory within the Born-Oppenheimer and dipole approximations. In the length gauge, they are given by

$$T^{\alpha,v,v'}_{p_1,q_1,h_1,l_1}(\mu_1,\omega) = \left(\frac{\alpha_s^3}{e^4}\frac{4}{3}\pi\right)^{1/2} \langle \psi_{\alpha,p_1,q_1,h_1,l_1}\chi_{\alpha,v'}|\hat{\epsilon}_{\mu_1}\cdot\mathbf{d}_{\mu_1}|\psi_0\chi_{0,v}\rangle \tag{1}$$

where α_s is the hyperfine constant, v and v' are the initial and final vibrational quantum numbers, e is the electron charge, ω is the photon energy which is related to the photoelectron energy ε_α through the equation $\varepsilon_\alpha = \hbar\omega$ - IE_α, where IE_α is the ionization energy required to produce a molecular cation in the α electronic state, ψ_0 is the initial electronic state, $\psi_{\alpha,p_1,q_1,h_1,l_1}$ is final electronic continuum states of the molecule that describes an ejected electron in the $(p_1q_1h_1l_1)$-th channel and a residual molecular ion in the α state, p_1 denotes the irreducible representation (IR) of the molecular point group under consideration, q_1 stands for a component of this representation if its dimensionality is greater than one, h_1 distinguishes between different bases of the same IR corresponding to the same value of the angular momentum of the escaping electron l_1, $\chi_{0,v}$ is the initial vibrational state, $\chi_{\alpha,v'}$ is the final vibrational state, $\mathbf{d}_{\mu_1}$ represents one of the following spherical components of the electronic dipole operator

$$d_{-1} = \frac{(d_x - id_y)}{\sqrt{2}} = d\times\left(\frac{4\pi}{3}\right)^{1/2} Y_{1,-1} \tag{2}$$

$$d_0 = d_z = d\times\left(\frac{4\pi}{3}\right)^{1/2} Y_{1,0} \tag{3}$$

$$d_1 = -\frac{(d_x + id_y)}{\sqrt{2}} = d\times\left(\frac{4\pi}{3}\right)^{1/2} Y_{1,1} \tag{4}$$

and ϵ_{μ_1} one of the spherical components of the polarization vector

$$\epsilon_{-1} = \frac{(\epsilon_x - i\epsilon_y)}{\sqrt{2}} \tag{5}$$

$$\epsilon_0 = \epsilon_z \tag{6}$$

$$\epsilon_1 = -\frac{(\epsilon_x + i\epsilon_y)}{\sqrt{2}} \tag{7}$$

In the length gauge $\mathbf{d} = \mathbf{r}$ and, therefore, $d = r$.

Using the above expression of the transition amplitudes, one can evaluate the vibrationally resolved angular distribution of electrons ejected into the solid angle $d\Omega_e$

from a molecule with fixed orientation in space defined by the solid angle $d\Omega_m$ (fully differential vibrationally-resolved photoionization cross section or MFPAD) as follows (see [47, 48] for details)

$$\frac{d^2\sigma_\alpha^{v,v'}(\omega)}{d\Omega_m d\Omega_e} = (-1)^\mu 3\pi \left(\frac{e^2}{\alpha_s\omega}\right)^2 \sum_{L=0}^{2l_{max}} \sum_{M=-L}^{L} A_{LM}^{\alpha,v,v'}(\Omega_m,\omega)\, Y_L^M(\Omega_e) \tag{8}$$

where

$$\begin{aligned} A_{LM}^{\alpha,v,v'}(\Omega_m,\omega) = & \sum_{p_1,q_1,h_1,l_1,m_1,\mu_1} \sum_{p_2,q_2,h_2,l_2,m_2,\mu_2} (-i)^{l_1-l_2} e^{i(\sigma_{l_1}(\omega)-\sigma_{l_2}(\omega))} (-1)^{m_1+\mu_1} \\ & \times \left(\frac{(2l_1+1)(2l_2+1)(2L+1)}{4\pi}\right)^{1/2} \begin{pmatrix} l_1 & l_2 & L \\ 0 & 0 & 0 \end{pmatrix} \begin{pmatrix} l_1 & l_2 & L \\ -m_1 & m_2 & M \end{pmatrix} \\ & \times b_{h_1,l_1,m_1}^{p_1,q_1} b_{h_2,l_2,m_2}^{*p_2,q_2} T_{p_1,q_1,h_1,l_1}^{\alpha,v,v'}(\mu_1,\omega)\, T_{p_2,q_2,h_2,l_2}^{\alpha,v,v'\,*}(\mu_2,\omega) \\ & \times \sum_\Lambda (2\Lambda+1) \begin{pmatrix} 1 & 1 & \Lambda \\ -\mu & \mu & 0 \end{pmatrix} \begin{pmatrix} 1 & 1 & \Lambda \\ -\mu_1 & \mu_2 & \mu_1-\mu_2 \end{pmatrix} \mathcal{D}_{\mu_1-\mu_2,0}^{\Lambda}(\Omega_m) \end{aligned} \tag{9}$$

l_{max} is the maximum l value, and $\mathcal{D}_{\mu_1-\mu_2,0}^{\Lambda}$ is a Wigner rotation matrix.

For linear polarization ($\mu = 0$) and randomly oriented molecules, the resulting vibrationally resolved cross section is given by

$$\frac{d\sigma_\alpha^{v,v'}(\omega)}{d\Omega_e} = \frac{\sigma_\alpha^{v,v'}(\omega)}{4\pi}\left[1+\beta_\alpha^{v,v'}(\omega)\, P_2(\cos\theta_e')\right] \tag{10}$$

where $\beta_\alpha^{v,v'}(\omega)$ is the vibrationally-resolved electron asymmetry parameter:

$$\beta_\alpha^{v,v'}(\omega) = \frac{\bar{A}_{L=2}^{\alpha,v,v'}(\omega)}{\bar{A}_{L=0}^{\alpha,v,v'}(\omega)} \tag{11}$$

$\bar{A}_L^{\alpha,v,v'}$ is the $A_{LM}^{\alpha,v,v'}$ function transformed back in the laboratory frame and integrated over all the possible orientations of the molecule:

$$\bar{A}_L^{\alpha,v,v'}(\omega) = \frac{1}{8\pi^2}\int \bar{A}_{LM}^{\alpha,v,v'}(\Omega_m',\omega)\, d\Omega_m' \tag{12}$$

$$\bar{A}_{LM}^{\alpha,v,v'}(\Omega_m',\omega) = \sum_{M'} A_{LM'}^{\alpha,v,v'}(\Omega_m,\omega)\, \mathcal{D}_{M'M}^{L\,*}(\Omega_m) \tag{13}$$

and $\sigma_\alpha^{v,v'}(\omega)$ is the integral vibrationally-resolved photoionization cross section given by

$$\sigma_\alpha(v,v_\alpha',\omega) = \pi\left(\frac{e^2}{\alpha_s\omega}\right)^2 \sum_{p_1,q_1,h_1,l_1,\mu_1} \left|T_{p_1,q_1,h_1,l_1}^{\alpha,v,v'}(\mu_1,\omega)\right|^2, \tag{14}$$

To evaluate the electronic continuum state $\psi_{\alpha,p_1,q_1,h_1,l_1}$, we use the extension of density functional theory described in Refs. [3, 21], which is based on original work developed by Decleva and coworkers to treat molecular ionization at the molecule's equilibrium position [49–52]. Since the method has been described in detail in Refs. [3, 21], here we only summarize the basic ingredients.

Briefly, in this method, bound and continuum electronic states are written as Slater determinants of Kohn-Sham orbitals calculated as follows. The first step consists in

performing a standard LCAO-DFT calculation (LCAO stands for linear combination of atomic orbitals) for the ground state of the molecule by using the program ADF *(Amsterdam Density Functional)*. In these ADF calculations, we use a double zeta plus polarization (DZP) basis set centered on each atom and a LB94 or LDA functional to describe exchange and correlation effects. The resulting ground state density is then used to build the hamiltonian matrix in a new basis set of B-spline functions B and real spherical harmonics Y^R:

$$\xi^i_{pqlhj}(r_i,\theta_i,\phi_i) = \frac{1}{r}B_j(r_i)\sum_{m=-l}^{l} b_{pqlhm}Y^R_{lm}(\theta_i,\phi_i) \tag{15}$$

where q represents a specific component of the p irreducible representation (IR), l and m correspond to the usual angular momentum quantum numbers, h counts the number of independent angular functions with a given l in the q component of the p IR, i indicates the ith non-equivalent expansion center, j refers to the jth B-spline, r_i, θ_i and ϕ_i stand for the spherical coordinates referred to the i center, and b_{pqlhm} are the coefficients of the symmetry adapted linear combination of real spherical harmonics.

The electronic wave functions are expanded over three centers: (i) the center of the molecule (denoted by the superscript 0), which is associated with a large sphere of radius R^0_{max} to correctly account for the long range behavior of the continuum wave functions; (ii) the positions occupied by the two nuclei (denoted by the superscript $i \neq 0$), which are associated with a small sphere of radius R^i_{max} to accurately describe the sharpness of the bound state wave functions. This radius is small ($\approx 1a.u.$) in order to avoid significant overlap with expansions performed on neighboring centers.

Thus, Kohn-Sham orbitals are written as

$$\varphi_{npq} = \sum_{j=1}^{N_b}\sum_{lh} c^0_{npqlhj}\xi^0_{pqlhj} + \sum_{i=1}^{\kappa}\sum_{j=1}^{N_b}\sum_{lh} c^i_{npqlhj}\xi^i_{pqlhj} \tag{16}$$

where κ is the number of atomic centers and N_b is the total number of B-spline functions. The unknown coefficients are determined by substituting the above equation in the well-known Kohn-Sham equations:

$$\hat{H}_{KS}\varphi_i = \varepsilon_i\varphi_i \quad i = 1, ..., N \tag{17}$$

where:

$$\hat{H}_{KS} = -\frac{1}{2}\nabla^2 + V_{eff}(\mathbf{r}) \tag{18}$$

and:

$$V_{eff}(\mathbf{r}) = -\sum_{i=1}^{\kappa}\frac{Z_i}{|\mathbf{r}-\mathbf{R}_i|} + V_H(\mathbf{r}) + V_{XC}(\mathbf{r}) \tag{19}$$

where $V_H(\mathbf{r})$ is the electrostatic Hartree potential and $V_{XC}(\mathbf{r})$ the exchange-correlation potential. Here we have used the LB94 functional, which reproduces quite well the photoelectron spectra. To evaluate the resulting integrals, a numerical three-dimensional Gauss-Legendre scheme has been employed. Kohn-Sham orbitals associated with bound

states are obtained by a generalized diagonalization of $\hat{H}_{KS}$ and those associated with continuum states by block inverse iteration of $\hat{H}_{KS}$ on a previously defined energy grid $\{E_k\}$ containing N_{E_k} points [53]. Dipole matrix elements are calculated for each partial wave, as a function of photoelectron energy and internuclear distance.

The vibrational wave functions are the solutions of the Schrödinger equation

$$\left[-\frac{1}{2\mu}\nabla_R^2 + E_\alpha(R) - W_{v_\alpha}\right]\chi_{\alpha,v_\alpha}(R) = 0, \tag{20}$$

where μ is the reduced mass of the molecule, $E_\alpha(R)$ the potential energy curve associated to the α electronic state of the neutral molecule or the cation, and W_{v_α} the total energy. In this equation, molecular rotation has been ignored because energy resolution in standard photoelectron spectroscopy measurements does not allow one to resolve the rotational structure. Equation (20) has been solved in a basis of 1000 B-splines within a box of 10 a.u.. The potential energy curves used in these calculations are the same as those described in Ref. [3].

3. Results and discussion

There are very few experimental data for vibrationally resolved angular distributions and most of them have been obtained for randomly oriented molecules. Thus, to gauge the quality of the present calculations, we first present results for randomly oriented molecules and then for fixed-in-space molecules for which there are no experimental data.

3.1. Randomly oriented molecules

In this section, we present the calculated vibrationally resolved electron asymmetry parameters for K-shell and valence-shell photoionization of N_2 (Fig. 1) and CO (Fig. 2) for photoelectron energies smaller than 60 eV. The results are compared with the available experimental data [4, 13, 27, 54]. In the case of valence-shell photoionization, a direct comparison over a wide range of photon energies can only be carried out with vibrationally averaged β parameters. Nevertheless, for the sake of completeness, in the last case we have also included in the figures our vibrationally resolved results. Fig. 3 shows a comparison between the calculated average β parameters and the experimental ones for K-shell photoionization.

As expected, for both N_2 and CO, the β parameter tends to a value close to 2 as the photon energy increases. A β value of 2 is associated to a perfect p-like electron angular distribution, which is what one would expect for an electron moving in the field of a perfectly spherical potential. Indeed, at very high energies, the escaping electron does not see the details of the two-center potential and, consequently, the resulting angular distribution should have an almost perfect atomic character. This is so unless the electron wavelength coincides or is of the order of the internuclear distance, where two-center interferences and diffraction effects are expected to occur (see next section).

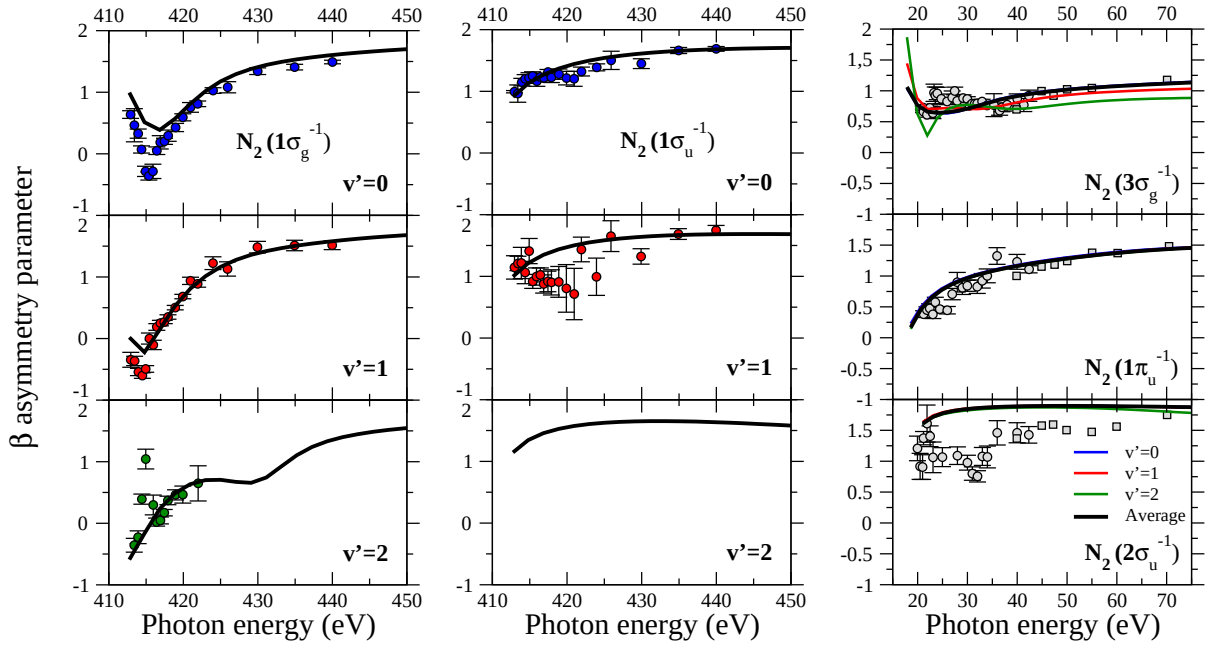

Figure 1. Vibrationally resolved electron asymmetry parameter, β, for N_2 photoionization from the $1\sigma_g$ (left panel), $1\sigma_u$ (central panel), and $3\sigma_g$, $1\pi_u$, and $2\sigma_u$ (right panel) molecular orbitals. Lines: present results. Circles in the left and central panels: experimental data from Ref. [13]. Circles in the right panel correspond to non vibrationally resolved experimental data: Refs. [54] (circles) and [55] (squares).

The latter effects are responsible for the oscillations that are observed in the β parameter as it approaches the value of 2 (see Fig. 4).

Figs. 1 and 2 show a very good agreement between the present results and the available experimental data. They are also in reasonable agreement with previous theoretical results obtained within the random-phase approximation [13, 27], although the latter are obtained by using a free parameter in the theory. As can be seen, the β parameters associated with different vibrational levels v' of the residual molecular cation are very similar. The largest variations with v' are observed for photoionization from the highest-occupied molecular orbital (HOMO), namely $N_2(3\sigma_g^{-1})$ and $CO(5\sigma^{-1})$. These are the orbitals where electron delocalization is more important. They also have several nodes along the internuclear axis. Consequently, one can reasonably expect that the electron angular distribution should be more sensitive to the particular range of internuclear distances probed by the different vibrational levels of the molecular cation. In particular, it can be seen that the larger v' the smaller the value of β, i.e., the less atom-like the angular distribution. This is due to the fact that, as v' increases, photoionization probes regions of increasingly larger values of R, hence the angular distribution has a less pronounced atomic character (i.e., β is far lower than 2).

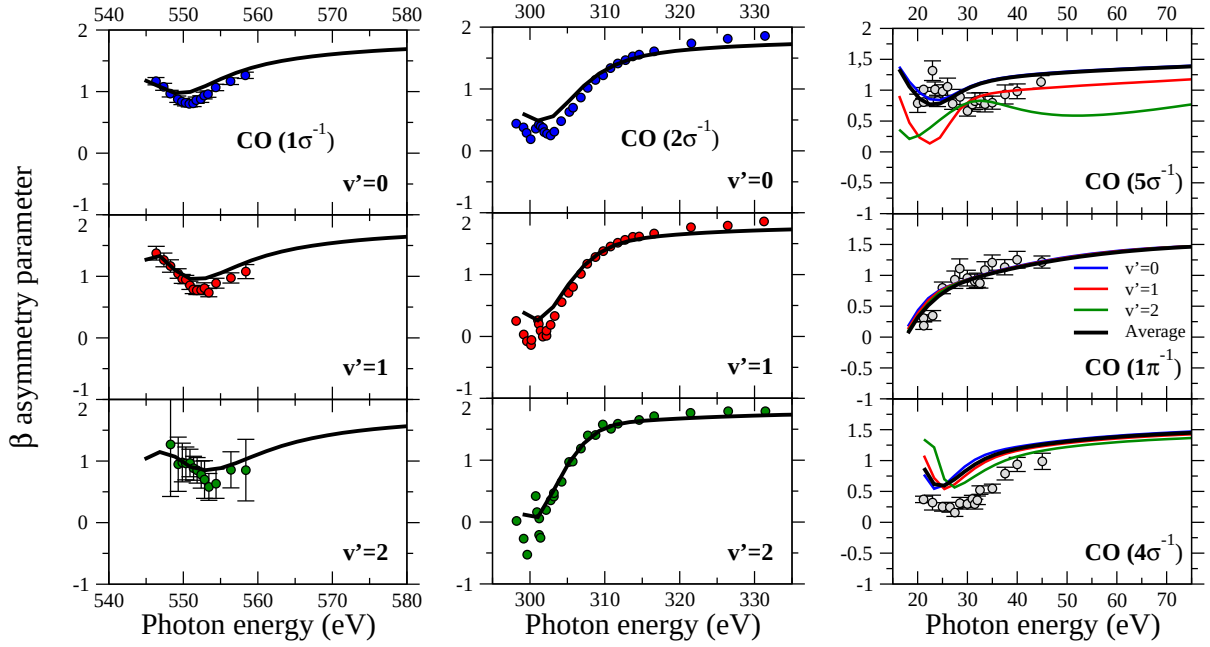

Figure 2. Vibrationally resolved electron asymmetry parameter, β, for CO photoionization from the 1σ (left panel), 2σ (central panel), and 5σ, 1π, and 4σ (right panel) molecular orbitals. Lines: present results. Circles in the left panel: experimental data from Ref. [27]. Circles in the central panel: experimental data from Ref. [4]. Circles in the right panel correspond to non vibrationally resolved experimental data: Ref. [54].

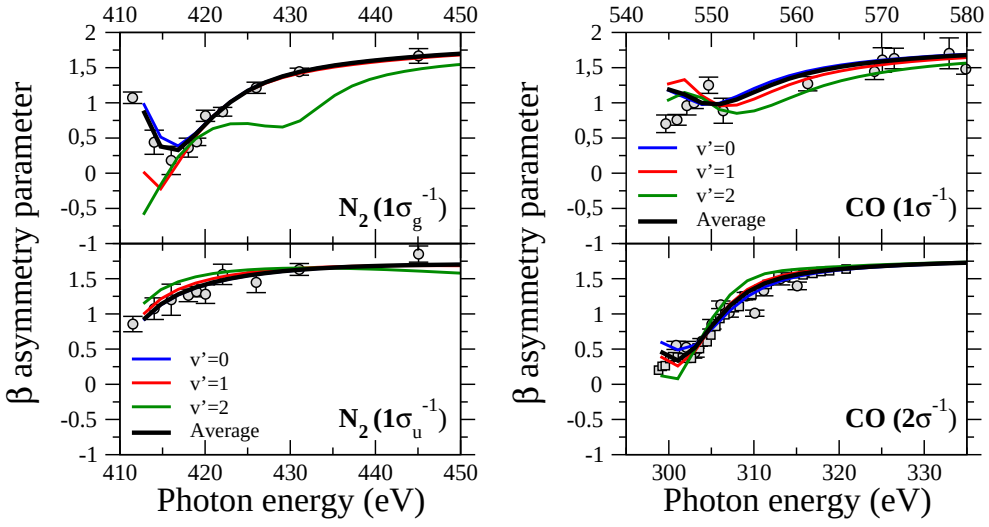

Figure 3. Vibrationally resolved electron asymmetry parameter, β, for N_2 photoionization from the $1\sigma_g$ and $1\sigma_u$ molecular orbitals (left panel), and for CO photoionization from the 1σ and 2σ molecular orbitals (right panel). Lines: present results. Experimental data in the left and right panels correspond to non vibrationally resolved experimental data from Refs. [38], and [56] (circles) and [57] (squares), respectively.

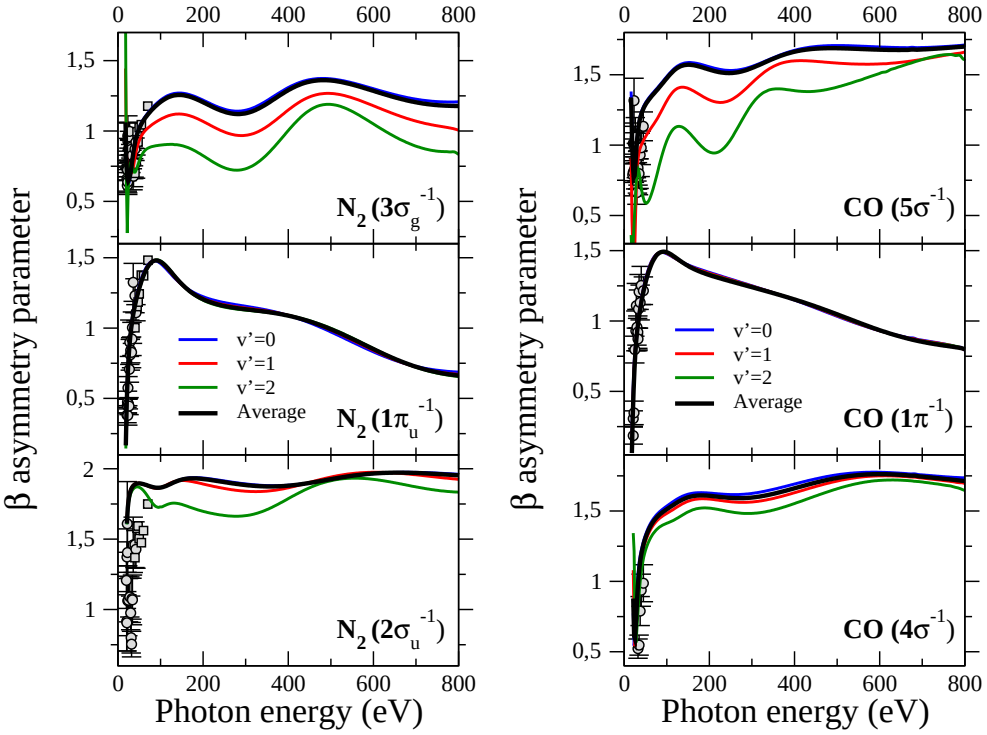

Figure 4. High photon-energy behavior of the vibrationally resolved electron asymmetry parameter, β, for N_2 photoionization from the valence molecular orbitals $3\sigma_g$, $1\pi_u$, and $2\sigma_u$ (left panel), and for CO photoionization from the valence molecular orbitals 5σ, 1π, and 4σ (right panel). Lines: present results. Experimental data in the left and right panels correspond to non vibrationally resolved experimental data from Refs. [54] (circles) and [55] (squares), respectively.

3.2. Fixed-in-space molecules

In this section we present vibrationally resolved MFPADs of N_2 and CO for two particular molecular orientations: parallel and perpendicular to the polarization direction of the incident light. These two orientations provide information for molecular states of Σ and Π symmetries, respectively. Figures 5 and 6 present our results for K-shell ionization of N_2 with parallel and perpendicular orientations, respectively, at five photon energies: 420, 550, 605, 699 and 750 eV. Only results for the final vibrational levels $v' = 0$ and $v' = 2$ are shown. To better understand the origin of the different structures observed in the MFPAD, the figures also include the total cross sections and partial-wave contributions as functions of photon energy. Due to symmetry considerations, only partial waves associated with odd values of the angular momentum lead to non zero contributions. In the parallel case (see Fig. 5), the $l = 3$ partial-wave contribution presents a pronounced minimum at around 600 eV for $v' = 0$ and at around 520 eV for $v' = 2$. The position of this minimum progressively shifts to lower energies at v' increases. Other partial waves also exhibit minima, although they are less pronounced and, in some cases, they lie very close to the ionization threshold. The origin of these

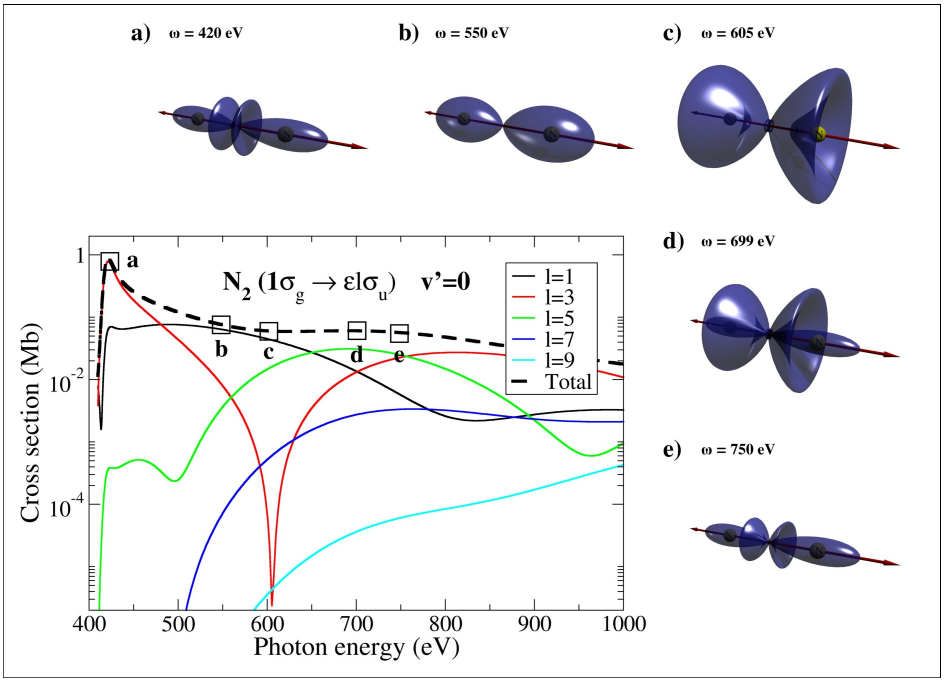

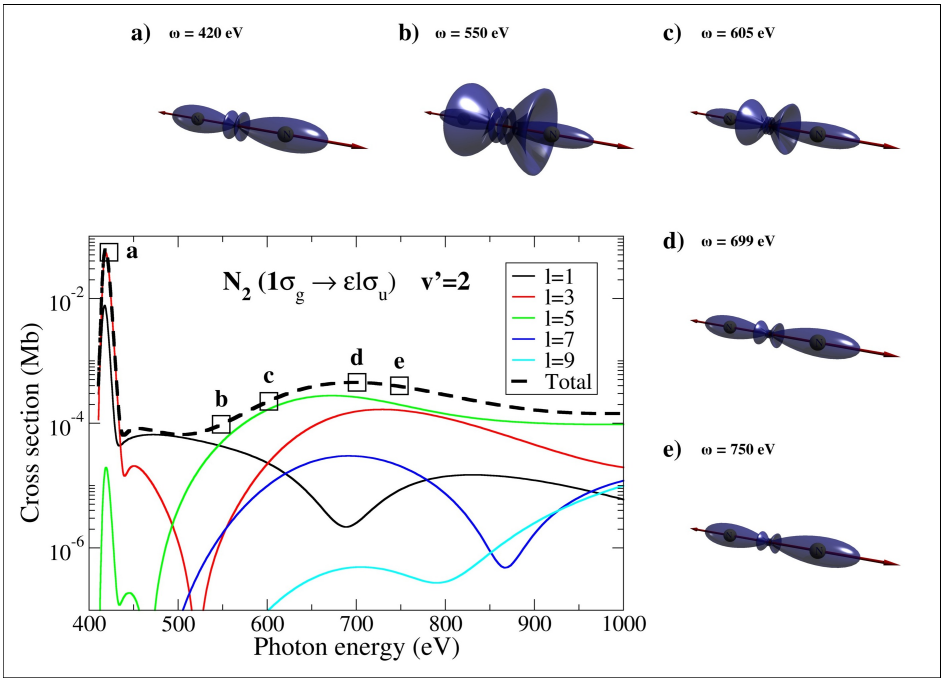

Figure 5. Vibrationally resolved molecular-frame photoelectron angular distributions (MFPAD) for $N_2(1\sigma_g^{-1})$ photoionization. Molecules are parallel to the polarization direction (indicated by a double arrow). The MFPADs are represented in the form of 3D polar plots for photon energies 420, 550, 605, 699 and 750 eV. Integrated total and partial photoionization cross sections as functions of photon energy are shown in a 2D box. Upper panel: $v' = 0$. Lower panel: $v' = 2$.

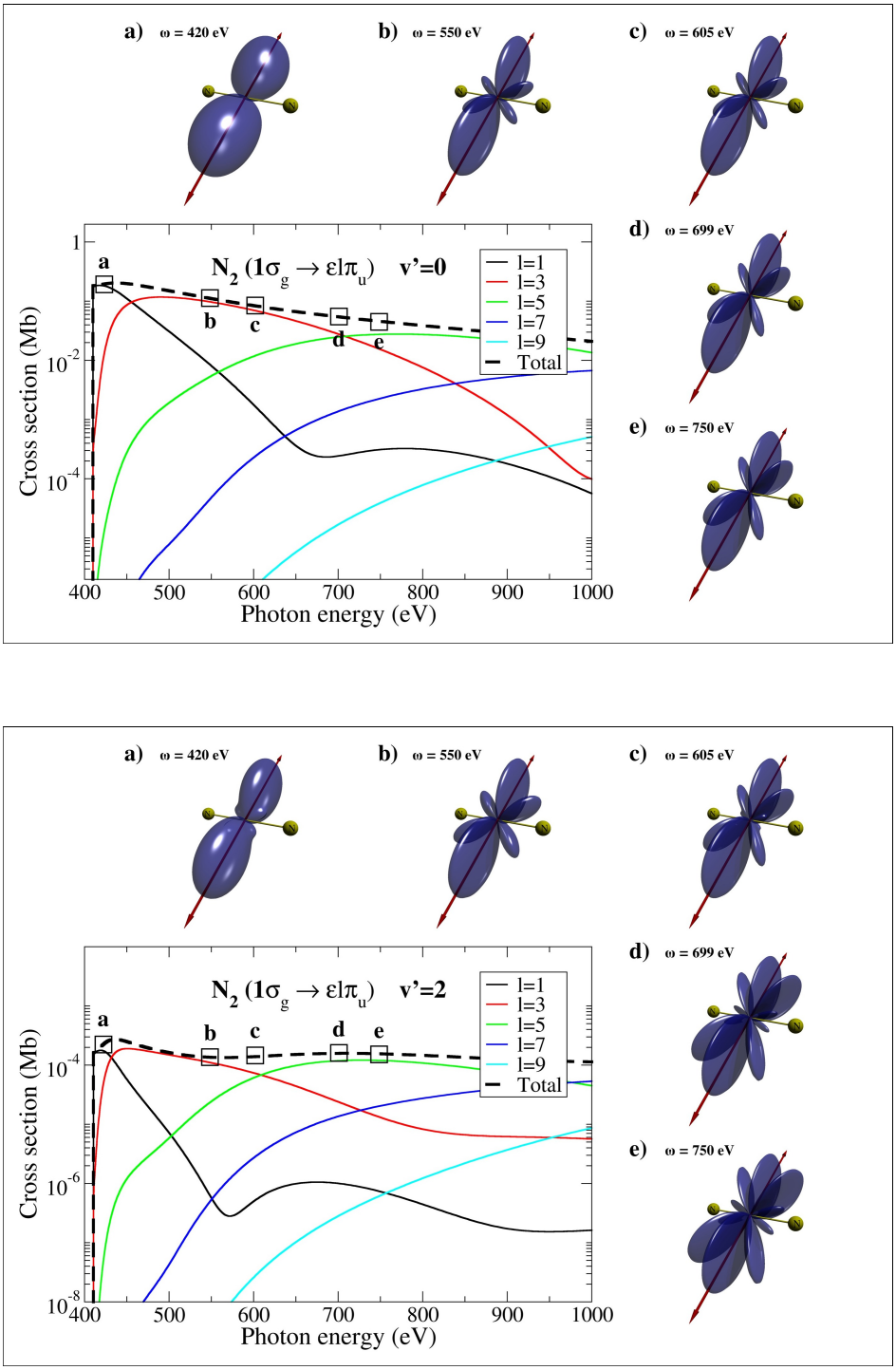

Figure 6. Same as figure 5 for molecules perpendicular to the polarization direction.

minima has been explained in Ref. [40, 42] in the context of H_2 photoionization as resulting from electron confinement in between the two nuclei. This is possible when the electron momentum k_e approximately satisfies the equation $k_e R = l\pi$, which is nothing else than the particle-in-a-box formula. Indeed, when the molecule is parallel

to the polarization direction, the electron is forced to move along the internuclear axis and, when its wavelength coincides or is approximately equal to the internuclear separation, it is transiently trapped and, consequently, does not follow the internuclear axis. This behavior can be clearly seen in the MFPAD for photon energies in the vicinity of the minimum of the $l = 3$ partial wave. In contrast, at lower and higher energies, the calculated MFPADs indicate that the electron escapes preferentially along the internuclear axis. For N_2, the equilibrium internuclear distance is $R_e = 2.07$ a.u. and the previous formula predicts that the lowest energy at which the minima should appear is approximately 30 eV above threshold for the $l = 1$ partial wave and 280 eV for the $l = 3$ one. The first one is so close to threshold that it is barely seen. Furthermore, at such low energy, the escaping electron is strongly perturbed by the remaining ionic core, which cannot be described by the above simple formula because it is only valid for a free electron. Thus, confinement is actually observed in the range of photoelectron energies between 200 and 300 eV, i.e., in the vicinity of the $l = 3$ minimum. It can be seen that, for $v' = 2$, confinement appears at lower photon energies than for $v' = 0$. This is because the actual internuclear distance that the escaping electron sees is intermediate between R_e and that of the remaining $N_2^+(v')$ cation, R'. As v' increases, the mean value of R' also increases due to the anharmonicity of the potential energy curves. Therefore, the electron momentum and energy at which confinement should be observed are smaller. This is similar to what has been observed in H_2 [40, 42]. It is worth stressing here that the minima observed in the different partial waves should not be called Cooper minima because the latter arise from cancellations in the dipole transition matrix elements that involve wave functions with one or several radial nodes. Since the $1\sigma_g$ orbital from which the electron escapes has no radial node, it is clear that this concept does not apply here.

In the perpendicular case (see Fig. 6) and at very low photon energy, the MFPADs are almost perfect dipole-like, which is the consequence of the dominance of the $l = 1$ partial wave and is what one would expect for a pure atomic system. In other words, the electron mainly follows the direction imposed by the electric field. As the photon energy increases, one can see the appearance of smaller satellite lobes whose magnitude progressively increases. The position of these lobes is approximately given by the simple formula $\sin\theta_e = n\lambda_e/R$, where θ_e is the angle between the main lobe perpendicular to the internuclear axis and the satellite lobes. This formula is identical to that used to explain the position of the interference peaks observed in the famous Young's double-slit experiment. A behavior similar to that observed in Fig. 6 has been reported in [40, 42] for the H_2 molecule. One can thus conclude that the observed angular patterns are due to the coherent emission of the electron from the two atomic centers in a direction perpendicular to the molecular axis. The above formula predicts that, as the photon energy increases, i.e., as λ_e decreases, there is an increasing number of n values compatible with the constraint $|\sin\theta_e| \leq 1$. This explains the appearance of more and more satellite lobes as the photon energy increases. The appearance thresholds for these satellite lobes as well as the angle they form with the dominant central lobe is also reasonably explained by this formula. As can be seen in Fig. 6, the appearance

thresholds depend on the final value of v'. Indeed, for $v' = 2$, the threshold energies associated with the different n values are lower than for $v' = 0$: for $v' = 2$, satellite lobes associated with $n = 2$ can be clearly seen at 700 eV, while, for $v' = 0$ they are absent at this energy. The explanation for the v' dependence is the same as that given in the previous paragraph: as v' increases, the mean value of R' also increases and the minimum energy (electron wavelength) required to open a new channel n is smaller (larger).

Figures 7 and 8 present our results for O($1s^{-1}$) ionization of CO with parallel and perpendicular orientations, respectively, at five photon energies: 549, 579, 620, 720 and 850 eV. The figures also include the total cross sections and partial-wave contributions as functions of photon energy. In this case no selection rule limits the number of contributing partial waves. The partial-wave contributions exhibit a very complex behavior, with maxima and minima that do not follow a simple pattern. The main difference with the N_2 case is that the initial orbital from which the electron is ejected is almost perfectly localized on the oxygen atom. Therefore, one cannot expect angular patterns associated with coherent emission from the two atomic centers as those observed for N_2. Instead, diffraction of the ejected electron by the neighboring carbon atom should leave its trace in the MFPADs. This should occur when the electron wavelength is comparable to the CO equilibrium internuclear distance, which is $R_e = 2.13$ a.u. and corresponds to a photoelectron energy of approximately 120 eV (i.e., a photon energy of 662 eV). So, according to this formula, one should observe scattering by the neighboring C atom at around this energy. In both the parallel and perpendicular cases, one can see that, around this photoelectron energy, the MFPAD is complex and exhibits lobes that point to both the C and O atoms, indicating that the electron coming from the O center is efficiently diffracted by the C center. In the parallel case the lobes are oriented along the molecular axis, while in the perpendicular case they are preferentially oriented in the normal direction. As the photon energy increases in the parallel case (Fig. 7), the MFPAD is more and more localized around the O atom, which reflects the fact that there is less and less diffraction by the neighboring C atom. In the perpendicular case (Fig. 7), the MFPAD becomes more and more dipole-like, as if it was a purely atomic angular distribution, and the additional satellite lobes progressively disappear. This is the opposite behavior to that observed in N_2 (see Fig. 6). The transition from the diffraction zone to the atom-like one occurs earlier for $v' = 2$ than for $v' = 0$, which is again the consequence of the effective internuclear distance increasing with v'.

4. Summary and conclusions

We have evaluated vibrationally resolved photoelectron angular distributions from randomly oriented and fixed-in-space N_2 and CO molecules by using an extension of the static-exchange density functional theory that includes the nuclear motion. Both K-shell and valence-shell photoionization have been considered. The results for randomly oriented molecules are in excellent agreement with experiment, while the absence of

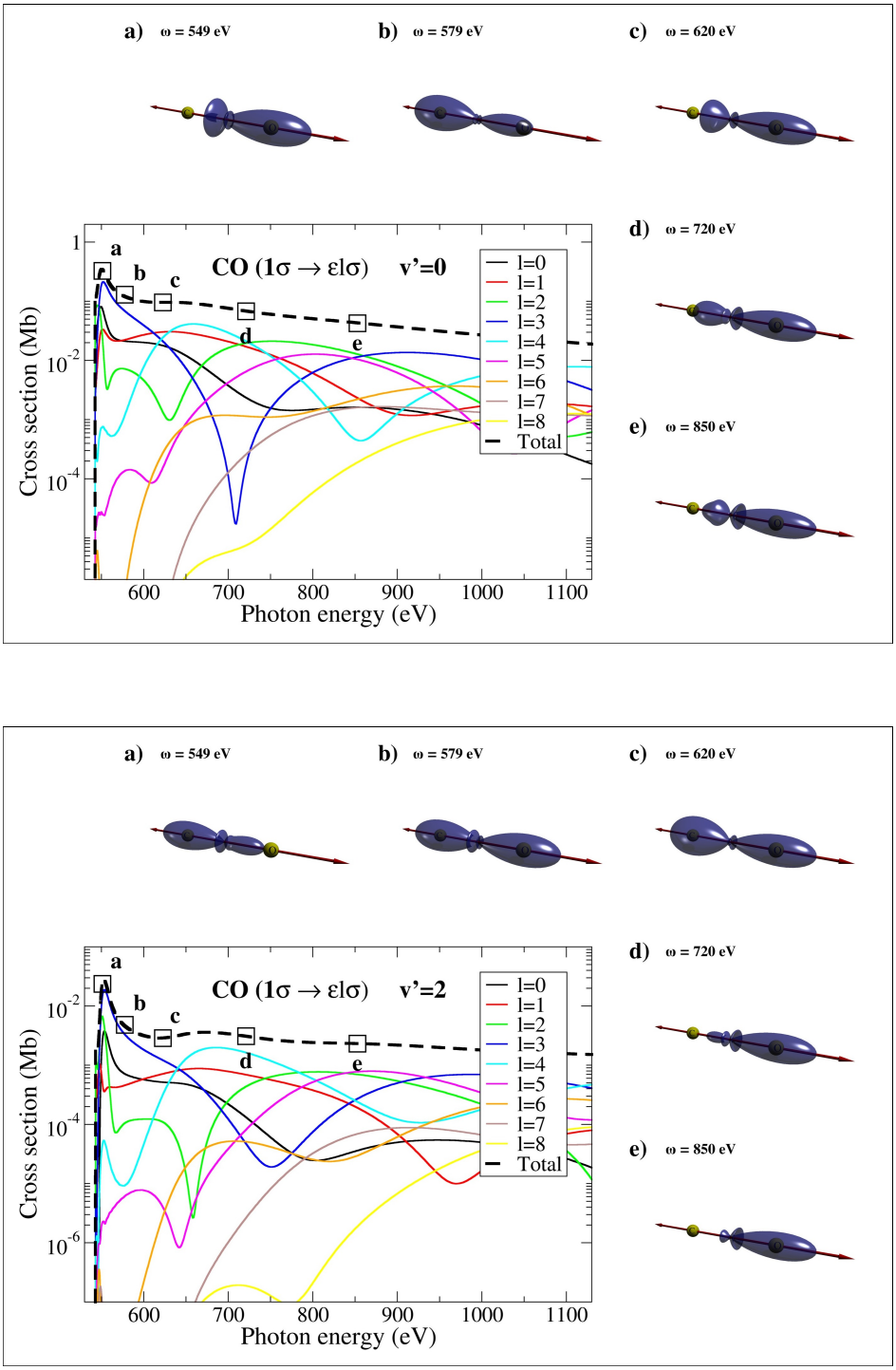

Figure 7. Vibrationally resolved molecular-frame photoelectron angular distributions (MFPAD) for CO($1\sigma^{-1}$) photoionization. Molecules are parallel to the polarization direction (indicated by a double arrow). The MFPADs are represented in the form of 3D polar plots for photon energies 549, 579, 620, 720 and 850 eV. Integrated total and partial photoionization cross sections as functions of photon energy are shown in a 2D box. Upper panel: $v' = 0$. Lower panel: $v' = 2$.

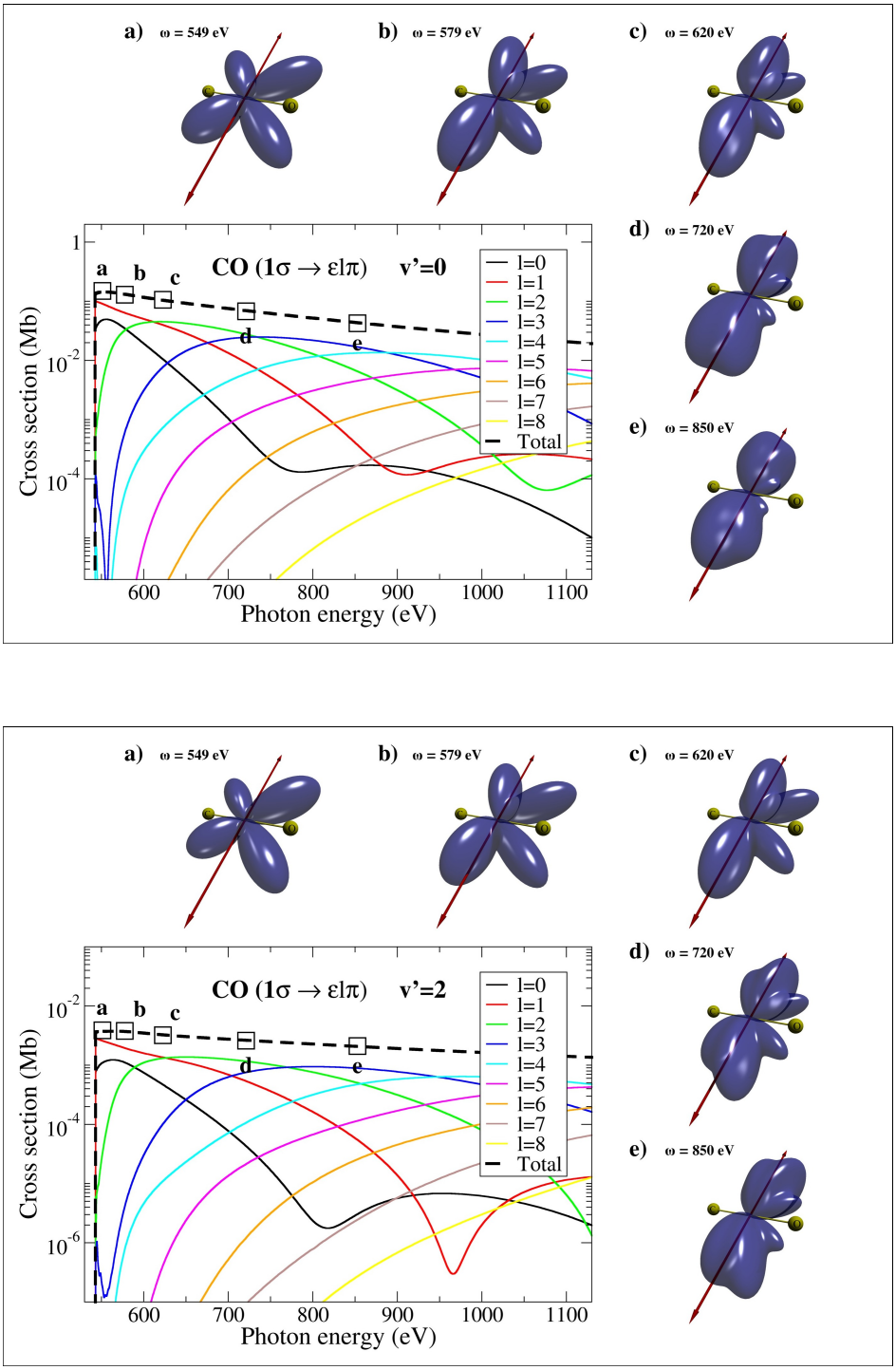

Figure 8. Same as figure 7 for molecules perpendicular to the polarization direction.

experimental data for fixed-in-space molecules gives our results a predictive value. Vibrationally resolved β parameters do not depend very much on the chosen vibrational level, except for the HOMO ionization channel, for which the higher the final vibrational state the lower the value of β. For fixed-in-space N_2 molecules, the MFPADs exhibit

the signature of electron confinement and coherent two-center interferences, similar to what has been found in H_2 photoionization [40, 42]. For fixed-in-space CO, they exhibit diffraction patterns resulting from the intramolecular scattering of an electron arising from a very localized area of the molecule. The conclusions reported in this work suggest that vibrationally resolved photoelectron angular distributions can be used to determine the structure of these simple molecules. Work along this line for the case of dissociative ionization is now in progress.

Acknowledgments

We thank Mare Nostrum BSC, Cineca and CCC-UAM for allocation of computer time. Work supported by the MICINN project Nos. FIS2010-15127, ACI2008-0777 and CSD 2007-00010 (Spain), the ERA-Chemistry project PIM2010EEC-00751, the European COST Action CM0702, the Marie Curie ITN CORINF, and the XCHEM Advanced Grant 290853 of the European Research Council.

References

[1] U. Hergenhahn, *Vibrational structure in inner shell photoionization of molecules*, J. Phys. B: At. Mol. Opt. Phys. **37** R89 (2004)

[2] E. D. Poliakoff and R. R. Lucchese, *Evolution of photoelectron vibrational coupling with molecular complexity*, Phys. Scripta **74** C71 (2006)

[3] E. Plésiat, P. Decleva and F. Martín, Phys. Chem. Chem. Phys. in press (2012)

[4] H. M. Köppe, A. L. D. Kilcoyne, J. Feldhaus and A. M. Bradshaw, *Relaxation effects in C1s photoionisation of CO: a high resolution photoelectron study in the near-threshold region*, J. Electron Spectrosc. Relat. Phenom. **75** 97 (1995)

[5] B. Kempgens *et al.*, *A high-resolution N 1s photoionization study of the N_2 molecule in the near-threshold region*, J. Phys. B: At. Mol. Opt. Phys. **29** 5389 (1996)

[6] U. Hergenhahn *et al.*, *Symmetry-Selective Observation of the N 1s Shape Resonance in N_2*, J. Phys. Chem. A **105** 5704 (2001)

[7] J.-i. Adachi *et al.*, *Shape-Resonance-Enhanced Vibrational Effects in the Angular Distributions of C 1s Photoelectrons from Fixed-in-Space CO Molecules*, Phys. Rev. Lett. **91** 16 163001 (2003)

[8] D. A. Mistrov *et al.*, *Vibrational effects on the shape resonance energy in the K-shell photoionization spectra of CO*, Phys. Rev. A **68** 2 022508 (2003)

[9] G. J. Rathbone *et al.*, *Vibrational branching ratios in photoionization of CO and N2.*, J. Chem. Phys. **120** 2 778 (2004)

[10] S. K. Semenov *et al.*, *Interplay of different partial waves on vibrationally resolved photoionization of the O K shell of the CO molecule*, Phys. Rev. A **70** 5 052504 (2004)

[11] S. K. Semenov *et al.*, *Interference modulation in the vibrationally resolved photoionization of the $1\sigma_g$ and $1\sigma_u$ core levels of the N_2 molecule*, J. Phys. B: At. Mol. Opt. Phys. **39** L261 (2006)

[12] M. Matsumoto *et al.*, *Vibrationally resolved C and O 1s photoelectron spectra of carbon monoxides*, Chem. Phys. Lett. **417** 89 (2006)

[13] S. K. Semenov *et al.*, *Vibrationally resolved photoionization of the $1\sigma_g$ and $1\sigma_u$ shells of N_2 molecule*, J. Phys. B: At. Mol. Opt. Phys. **39** 375 (2006)

[14] X.-J. Liu *et al.*, *Young's double-slit experiment using core-level photoemission from N_2: revisiting CohenFano's two-centre interference phenomenon*, J. Phys. B: At. Mol. Opt. Phys. **39** 4801 (2006)

[15] A. A. Pavlychev, *C K-shell absorption and single-hole ionization in the CO molecule in the vicinity of the shape resonance*, J. Phys. B: At. Mol. Opt. Phys. **32** 2077 (1999)

[16] N. A. Cherepkov *et al.*, *O K-shell photoemission of the CO molecule: comparison between theory and experiment*, J. Phys. B: At. Mol. Opt. Phys. **37** 4803 (2004)

[17] A. A. Pavlychev and D. A. Mistrov, *Spectral distributions of vibrational excitations accompanying 1s shell photoionization in small molecules*, J. Phys. B: At. Mol. Opt. Phys. **42** 5 055103 (2009)

[18] S. K. Semenov, N. A. Cherepkov, T. Jahnke and R. Dörner, *Theoretical study of vibrationally resolved photoionization for the C K-shell of the CO molecule*, J. Phys. B: At. Mol. Opt. Phys. **37** 1331 (2004)

[19] B. Leyh and G. Raseev, *Theoretical study of electronic autoionization in CO: Vibrationally resolved results between 17 and 18.3 eV*, Phys. Rev. A **34** 4 2920 (1986)

[20] F. Gel'mukhanov *et al.*, *Youngs double-slit experiment using two-center core-level photoemission: Photoelectron recoil effects*, J. Electron Spectrosc. Relat. Phenom. **156-158** 265 (2007)

[21] S. E. Canton *et al.*, *Direct observation of Young's double-slit interferences in vibrationally resolved photoionization of diatomic molecules*, Proc. Natl. Acad. Sci. **108** 18 7302 (2011)

[22] L. Argenti *et al.*, *Double-slit experiment with a polyatomic molecule: vibrationally resolved C 1s photoelectron spectra of acetylene*, New J. Phys. **14** 033012 (2012)

[23] E. Plésiat *et al.*, *Intramolecular electron diffraction in vibrationally resolved K-shell photoionization of methane*, Phys. Rev. A to be published (2012)

[24] J. A. Stephens, D. Dill and J. L. Dehmer, *Vibrational branching ratios and photoelectron angular distributions in 5σ photoionisation of CO*, J. Phys. B: At. Mol. Opt. Phys. **14** 3911 (1981)

[25] N. A. Cherepkov and S. K. Semenov, *New Developments in the Theory of Molecular K-Shell Photoionization*, Int. J. Quantum Chem. **107** 2889 (2007)

[26] M. E. Smith, D. L. Lynch and V. McKoy, *Resonance effects in the 5σ photoionization of CO*, J. Chem. Phys. **85** 11 6455 (1986)

[27] S. K. Semenov *et al.*, *Vibrationally resolved photoionization of the O K-shell of CO molecule*, J. Electron Spectrosc. Relat. Phenom. **144-147** 211 (2005)

[28] J. L. Dehmer, D. Dill and S. Wallace, *Shape-Resonance-Enhanced Nuclear-Motion Effects in Molecular Photoionization*, Phys. Rev. Lett. **43** 14 1005 (1979)

[29] B. Basden and R. R. Lucchese, *Vibrationally resolved cross sections and asymmetry parameters for the photoionization of N_2 with coupling between the $(3\sigma_g)^{-1}$ and the $(2\sigma_u)^{-1}$ channels*, Phys. Rev. A **37** 1 89 (1988)

[30] B. E. Cole *et al.*, *Wavelength and vibrational-state dependence of photoelectron angular distributions. Resonance effects in 5σ photoionization of CO*, J. Chem. Phys. **72** 11 6308 (1980)

[31] R. M. Holmes and G. V. Marr, *The angular distribution of photoelectrons from N_2 , O_2 and CO as a function of photon energy*, J. Phys. B: At. Mol. Opt. Phys. **13** 945 (1980)

[32] M. R. F. Siggel *et al.*, *Resonance effects in the $5\sigma^{-1}$ photoionization channel of CO*, J. Chem. Phys. **96** 10 7433 (1992)

[33] J. E. Hardis *et al.*, *Autoionization dynamics in the valence-shell photoionization spectrum of CO*, J. Chem. Phys. **89** 2 812 (1988)

[34] H. M. Köppe *et al.*, *Autoionisation of doubly excited states in the C 1s photoexcitation of CO*, Chem. Phys. Lett. **260** 223 (1996)

[35] S. H. Southworth, A. C. Parr, J. E. Hardis and J. L. Dehmer, *Channel coupling and shape resonance effects in the photoelectron angular distributions of the $3\sigma_g^{-1}$ and $2\sigma_u^{-1}$ channels of N_2*, Phys. Rev. A **33** 2 1020 (1986)

[36] J. B. West *et al.*, *Branching ratios and photoelectron angular distributions through the Hopfield bands in N_2 between 650 and 730 Å*, J. Phys. B: At. Mol. Opt. Phys. **14** 1791 (1981)

[37] B. Zimmermann *et al.*, *Localization and loss of coherence in molecular double-slit experiments*, Nature Physics **4** 649 (2008)

[38] D. Rolles *et al.*, *Isotope-induced partial localization of core electrons in the homonuclear molecule N2.*, Nature **437** 711 (2005)

[39] C. J. Davisson, *The discovery of electron waves*, Nobel Lecture 387 (1937)
[40] J. Fernández, O. Fojón, A. Palacios and F. Martín, *Interferences from Fast Electron Emission in Molecular Photoionization*, Phys. Rev. Lett. **98** 4 043005 (2007)
[41] U. Becker, *Matter-wave interference made clear*, Nature **474** 586 (2011)
[42] J. Fernández, O. Fojón and F. Martín, *Double-slit, confinement, and non-Franck-Condon effects in photoionization of H_2 at high photon energy*, Phys. Rev. A **79** 2 023420 (2009)
[43] F. Heiser *et al.*, *Demonstration of Strong Forward-Backward Asymmetry in the C1s Photoelectron Angular Distribution from Oriented CO Molecules*, Phys. Rev. A **79** 13 2435 (1997)
[44] A. L. Landers *et al.*, *Photoelectron Diffraction Mapping: Molecules Illuminated from Within*, Phys. Rev. Lett. **87** 1 013002 (2001)
[45] T. Jahnke *et al.*, *Vibrationally Resolved K-shell Photoionization of CO with Circularly Polarized Light*, Phys. Rev. Lett. **93** 8 083002 (2004)
[46] M. S. Schöffler *et al.*, *Ultrafast probing of core hole localization in N_2*, Science **320** 920 (2008)
[47] N. Chandra, *On the theories of photoemission processes in diatomic molecules*, Chem. Phys. **108** 301 (1986)
[48] N. Chandra, *Photoelectron spectroscopic studies of polyatomic molecules: I. Theory*, J. Phys. B: At. Mol. Opt. Phys. **20** 3405 (1987)
[49] M. Stener *et al.*, *Response function study of CO photoionization: ab initio SCF and density functional results*, Chem. Phys. **272** 1 15 (2001)
[50] M. Stener, G. De Alti and P. Decleva, *Convergence of the density functional one-centre expansion for the molecular continuum : N_2 and $(CH_3)_3N$*, Theor. Chem. Acc. **101** 247 (1999)
[51] M. Stener and P. Decleva, *Time-dependent density functional calculations of molecular photoionization cross sections: N_2 and PH_3*, J. Chem. Phys. **112** 24 10871 (2000)
[52] M. Stener, G. Fronzoni and P. Decleva, *Time dependent density functional study of the symmetry resolved N 1s photoionization in N_2*, Chem. Phys. Lett. **351** 469 (2002)
[53] H. Bachau *et al.*, *Applications of B-splines in atomic and molecular physics*, Rep. Prog. Phys. **64** 1815 (2001)
[54] G. V. Marr, J. M. Morton, R. M. Holmes and D. G. McCoy, *Angular distribution of photoelectrons from free molecules of N_2 and CO as a function of photon energy*, J. Phys. B: At. Mol. Opt. Phys. **12** 43 (1979)
[55] F. A. Grimm and T. A. Carlson, *Angular distribution for the major photoelectron bands of nitrogen below 45eV binding energy*, Chem. Phys. **80** 389 (1983)
[56] C. M. Truesdale *et al.*, *Core-level photoelectron and Auger shape-resonance phenomena in CO, CO_2, CF_4, and OCS*, J. Chem. Phys. **80** 6 2319 (1984)
[57] M. Schmidbauer *et al.*, *Strong multi-electron excitations in the C 1s photoionization of CO and CO_2*, Chem. Phys. Lett. **199** 1 119 (1992)